Commissioning the DRAGON facility at ISAC

S. Engel [a], D. Hutcheon [b,1], S. Bishop [c,2], L. Buchmann [b], J. Caggiano [b,c], M.L. Chatterjee [d], A.A. Chen [c,3], J. D'Auria [c], D. Gigliotti [e], U. Greife [f], D. Hunter [c], A. Hussein [e], C.C. Jewett [f], A.M. Laird [b,4], M. Lamey [c,5], W. Liu [c], A. Olin [b], D. Ottewell [b], J. Pearson [g], C. Ruiz [c], G. Ruprecht [b], M. Trinczek [b], C. Vockenhuber [c] and C. Wrede [c,6]

[a] *Ruhr-Universität, Bochum, Germany*

[b] *TRIUMF, 4004 Wesbrook Mall, Vancouver, BC, Canada*

[c] *Simon Fraser University, Burnaby, BC, Canada*

[d] *Saha Institute of Nuclear Physics, Calcutta, India*

[e] *University of Northern British Columbia, Prince George, BC, Canada*

[f] *Colorado School of Mines, Golden, CO 80401, USA*

[g] *McMaster University, Hamilton, ON, Canada*

Abstract

The performance of the DRAGON recoil spectrometer at TRIUMF-ISAC has been studied using radiative capture reactions with stable beams of ^{12}C, ^{20}Ne, ^{21}Ne, ^{23}Na, ^{24}Mg and ^{26}Mg. Calibration of the deflection magnet measuring the beam energy was established and the beam suppression factors of the separator were investigated. Yields from six narrow resonances were measured and compared with previous results. For the 1112.6 keV resonance in ^{20}Ne(p,γ)^{21}Na our result is in disagreement with the NACRE database assignment but agrees with one other previous result.

[1] Corresponding author: hutcheon@triumf.ca

[2] Present address: Heavy Ion Nuclear Physics Lab, RIKEN, 2-1 Hirosawa, Wakoshi, Saitama 351-0198,Japan

[3] Present address: McMaster University, Hamilton, ON, Canada

[4] Present address: University of York, York, England

[5] Present address: Notre Dame University, South Bend, IN, USA

[6] Present address: Yale University, New Haven, CT 06510, USA

PACS: 29.0
Keywords: Nuclear astrophysics; Radiative capture; Mass separator.

1 INTRODUCTION

The DRAGON facility at TRIUMF-ISAC has been designed, constructed and used to study radiative capture involving unstable beams, with the goal of measuring reaction rates of interest during explosive hydrogen burning in stars. Many stellar rates are dominated by contributions from a small number of narrow resonances at relatively low energies (100's of keV) and typical lab reaction rates are less than 10^{-10} of the beam intensity. The low reaction probabilities, coupled with limited intensity of unstable beams (typically 10^7 to 10^9 s^{-1}), require the facility to have good detection efficiency and good rejection of beam particles. Exponential dependence of the stellar rate on resonance energy requires an accurate measurement of beam energies.

The design of DRAGON and performance of its detectors have been described in Ref. [1]. The four main components of DRAGON are: a differentially-pumped windowless gas target; a 30-element BGO gamma-ray detector array closely surrounding the gas target cell; a 21-m long mass separator containing magnetic and electric dipoles in two independent stages; end detectors to identify recoil ions. A schematic representation of the DRAGON layout is given in Fig. 1.

We report here the results of stable-beam commissioning runs which investigated the accuracy with which beam energy could be measured and the efficiency of the separator/detector system. Many of these measurements were performed as part of the Ph.D. thesis of S. Engel [2].

2 RESONANCE ENERGY

The contribution to stellar reaction rate from a narrow resonance depends linearly upon the resonance strength $\omega\gamma$ but exponentially upon the resonance energy E_R. An error ΔE in resonance energy leads to an error in calculated reaction rate by a factor $e^{\Delta E/kT}$, with T the temperature of the astrophysical environment. For example, at T = 0.2 GK an error ΔE = 5 keV produces a 33% error in calculated reaction rate for the resonance. Therefore, an important property of the DRAGON facility is the accuracy with which beam energy and energy loss in the gas target can be measured.

The separator produces a focus at the charge selection slits following the first magnetic dipole MD1 (see Fig. 1). The dispersion at these slits is -3.0 mm per 1% change in beam energy, allowing the beam energy after the gas target to be calculated from the MD1 magnetic field required to centre the beam on the slits. Because the lateral position of the beam at the gas target

affects beam position at the slits (linear magnification -0.44), a consistent method of beam centring is required. In early commissioning runs, the beam was centred in the 6-mm entrance aperture of the gas cell by deflecting the beam with an upstream steering magnet until the transmitted beam intensity dropped to 50% of the maximum, to both left and right; the beam was centred by setting the steering magnet to the average of the two 50%-transmission values. More recently, the centring is accomplished by viewing the light emitted by the passage of beam through the gas target, in a CCD camera mounted downstream of MD1 on the zero-degree axis. Beam direction is adjusted until the beam is not steered by the first pair of quadrupoles.

The usual method of determining the resonance energy with a thick solid target is to vary the beam energy to find the point at which the yield drops to 50% of the peak (plateau) yield. With the windowless gas target the interpretation of the yield curve is more complicated because the target is extended and detection efficiency drops when the resonance takes place in the most-upstream part of the gas. Rather than measuring yield vs beam energy, it is possible to correlate beam energy with gas cell pressure: as the beam energy is decreased the gas cell pressure also is reduced to maintain the resonance position at the mid-way point of the gas cell. The calibration point is found by the extrapolation to zero pressure in a plot of cell pressure vs MD1 field as measured by a calibrated nuclear magnetic resonance (NMR) probe (Fig. 2). The resonance position is deduced from the hit pattern in the BGO array.

The expression relating the MD1 magnetic field (B), the radius of curvature of the central ray (ρ_m), the charge state (q), the atomic mass unit u=931.49 MeV/c^2 and the atomic mass (A) to the kinetic energy (E) is

$$E/A = c_{mag}(\frac{qB\rho_m}{A})^2 - \frac{1}{2uc^2}(E/A)^2 \qquad (1)$$

Assuming ρ_m to have its design value of 1 m, the constant c_{mag} takes the value 48.24 (MeV/u)(T·m)$^{-2}$. The second term in Eq. 1, a relativistic correction, is never larger than 0.1% for beam energies at DRAGON.

The results shown in Fig. 2 have been combined with the resonance energies obtained in previous experiments, using Eq. 1 to calculate the magnet constant c_{mag} for comparison with the design value of 48.24 (MeV/u)(T·m)$^{-2}$. Atomic masses were taken from Ref. [3] and corrected for the charge state of the beam ions.

The results (Table 1) suggest a magnet effective length 0.05% shorter than the design value. Possible variation of MD1 effective length with field strength was investigated by measuring the fields required to bend various charge states of a ^{24}Mg beam. Table 2 shows the results. There is a small, systematic change

in q·B with increasing field at a level of ≈0.5%/T. The effect may be due to a change in magnet effective length or small variation of energy loss through the gas target according to the charge state of the exiting ion.

Within measurement uncertainties of ≈1 keV/u, resonance energies for other (p,γ) and (α,γ) reactions calculated using the design value for the magnet constant, c_{mag}=48.24, have been in accord with literature values. Of particular interest was an energy scan around the threshold of the ^{24}Mg(p,γ)^{25}Al resonance at 214.0 keV, which served to demonstrate a 5 keV error in the accepted reaction Q-value of the ^{21}Na(p,γ)^{22}Mg reaction [6]. Recent re-measurements of the mass and excited-state energies of ^{22}Mg have confirmed the revised Q-value [7–9].

A notable exception has been the pair of resonances near 500 keV/u in ^{21}Ne(p,γ). We observe resonance thresholds ≈5 keV/u lower than the 500 and 521 keV/u found by Anttila *et al.* [10]. Therefore, as a further check of our magnet calibration, we measured NMR vs target gas pressure for the ^{23}Na(p,γ)^{24}Mg resonance at an energy E=508.0±0.1 keV/u [11]. The extrapolation to zero pressure gave a magnet constant 48.225±0.026 (MeV/u)(T·m)$^{-2}$, confirming the earlier calibration.

3 BACKGROUND SUPPRESSION

Radiative capture reactions of interest for nuclear astrophysics usually are weak, with typical reaction yields per incident beam particle being in the range 10^{-10} down to 10^{-15}. In inverse kinematics, the heavy recoil ions emerge with nearly the same momentum and direction as beam ions. The ability of the separator and detectors to suppress beam background, with efficient detection of desired reaction products, is illustrated with examples from both stable and radioactive beam experiments. The suppression factor is the ratio of the number of beam particles incident on the target divided by the number of beam particles which satisfy all hardware coincidences and software cuts that are required to define a valid capture event.

3.1 The gamma-ray detectors

The array of 30 BGO scintillators detects gamma rays from radiative capture with an efficiency of order 40–50% per gamma ray, in the typical case where the requirement is simply that at least one member of the array collects one-half or more of the total energy. Detecting a gamma ray in coincidence with the recoil ion provides beam suppression which is limited only by the rate

of random background in the BGO array. Valid times-of-flight of recoil ions through the separator may vary by as much as 100 ns, corresponding to an accidental coincidence probability of 10^{-7}R, where R is the background rate (s^{-1}) in the BGO array. If the background is not time-correlated with the pulsed beam (86 ns between beam bursts), a further suppression factor of 5–10 is obtained by requiring gamma rays to be detected at the correct phase relative to the accelerator r.f.

In these stable-beam measurements, the random background rates were typically less than 100 s^{-1}, resulting in gamma–recoil coincidence spectra which were background-free. With radioactive beams the BGO rates may be much higher due to beam-spill at the gas target: trigger rates were observed in the range 500–5000 s^{-1} for ^{21}Na beams of intensity up to 10^9 s^{-1}, with a corresponding reduction in the suppression factor provided by detection of gamma rays.

3.2 The mass separator

The dispersions at the Mass and Final slits of the separator are -0.47 and -1.8 cm per percent difference in the mass-to-charge ratio A/q (Table 2 of ref. [1]. It is expected that the beam suppression factor will be sensitive to both the quality of the beam focus at the slits and the difference in A/q between beam and desired recoil product. The beam background in proton capture experiments is much different from the background observed in alpha capture.

In proton capture, the beam ions closest in A/q to the recoil product are those having the same charge, q. The "leaky beam" which reaches the recoil-ion detectors has nearly the same energy as the beam that emerges from the gas target (Fig. 7 of ref. [12]). For the same reaction at different resonance energies, leaky beam suppression is found to increase rapidly with increasing beam energy, as illustrated in Fig. 3.

With the separator tuned for proton capture, transmission of unwanted beam is ascribed to the interaction of beam ions with target gas or residual gas in the separator. The energy dependence reflects that of Coulomb scattering or charge-changing collisions; beam emittance also becomes smaller as the energy increases. Because the recoil ions have slightly lower energy than the beam, the low-energy tail of the leaky-beam peak obscures the recoils of interest when the yield is much lower than the beam transmission factor. At a given beam velocity there can be order-of-magnitude variation in suppression of unwanted beam, which is believed to be related to variation in the spot-size and position of the beam at the gas target.

In alpha capture, the beam ions closest in A/q to the recoils are lower in charge than the selected recoils; for example a ^{12}C beam in charge state 4 will be nearest in A/q to ^{16}O recoils of charge 5. Transmitted beam particles are degraded from full beam energy, to make their electromagnetic rigidities closer to the separator tune. With the separator tuned for q=6 recoils from the $^{12}C(\alpha,\gamma)^{16}O$ reaction at 1.22 MeV/u, beam suppression was $\approx 1\times10^{13}$ with leaky beam appearing in groups at several energies, all well below the energy of recoil ions.

3.3 The recoil ion detectors

Several properties may distinguish the recoil ions from the unwanted beam which reaches the end-station detector: energy, energy-velocity correlation, rate of energy loss vs energy, radioactive decay mode. The usefulness of a property, and thus the best choice of recoil-ion detector, will vary according to the beam purity and energy, the reaction strength and the ratio of masses and atomic numbers of recoil vs beam ions. Many of the resonances of astrophysical interest are at low centre-of-mass energies, where background suppression is most challenging: separator transmission of leaky beam is higher, $\Delta E - E$ discrimination is difficult and fractional energy resolution of detectors is poorest. On the other hand, fractional resolution in time-of-flight (TOF) usually improves as the ion energy decreases.

The initial radiative capture programme at DRAGON mostly used a double-sided silicon strip detector and, when necessary, coincidence detection of gamma rays. At 1 MeV/u and above, the strip detector very effectively separated leaky beam from recoils on the basis of measured energies, but at 0.5 MeV/u the additional rejection by a simple energy cut is only a factor 5–10 (Fig. 4). At 0.2 MeV/u, separation no longer is possible (see Fig. 7 of [12]). For future studies of low-yield, low-energy reactions, systems better able to reject leaky beam ions are under study. Figure 5 illustrates a case of leaky-beam rejection by local TOF measurement [13]. The flight times of leaky beam and recoil ions from the ^{21}Ne(p,γ)^{22}Na resonance at 269 keV/u were measured using a micro-channel plate detecting secondary electrons from a thin C foil to provide a Start signal and a photo-multiplier tube viewing a plastic scintillator for the Stop. The TOF resolution was ≈550 ps FWHM, equivalent to an energy resolution of 1.8%, a substantial improvement over the resolution of the silicon strip detector under these conditions. It should be noted that the data were obtained at a pressure of only 0.76 Torr in the hydrogen gas target, so that the number of ^{22}Na ions may have been less than the thick-target yield.

Recoil ions cannot be distinguished from beam ions of the same velocity by using TOF. The product of ion energy and the square of its TOF, proportional

to the ion mass, can provide the necessary separation provided the energy can be measured with sufficient accuracy. We plan to investigate a system in which both the Start and Stop signals come from foil/MCP and the energy is measured in a gas ionization chamber, for use with ions of energies 0.2 MeV/u and lower.

4 CAPTURE REACTION YIELD MEASUREMENTS

Comparison with previously measured resonant capture strengths provides checks on many aspects of system performance. A number of stable-beam resonant-capture reactions were studied as a test of DRAGON's efficiency. Their salient features are summarized in Table 3. The uncertainties assigned to tabulated radiative capture strengths should be treated with caution: the recommended [16] strength for the 790.4 keV resonance in ^{24}Mg(p,γ)^{25}Al, 532±41 meV, is an evaluation of results which increased from 220±44 meV to 370±60 meV to 490±70 meV to 580±60 meV over a span of 24 years; two discordant values have been obtained for the 1112.6 keV resonance in ^{20}Ne(p,γ)^{21}Na reaction; there was only one previous measurement of the resonance in ^{21}Ne(p,γ)^{22}Mg at 258.6 keV.

Determination of yield requires good knowledge of beam normalization, stopping power of the target, gamma–ray detector efficiency, separator acceptance, charge state distributions of recoil ions, and recoil–ion detector efficiency. The narrow-resonance yield of capture recoils in charge state q, per incident beam ion, is

$$Y_q = \frac{\lambda^2}{2}\omega\gamma\frac{m_p + m_t}{m_t}\frac{F_q}{\epsilon} \tag{2}$$

where λ is the c.m. de Broglie wavelength, $\omega\gamma$ the resonance strength, m_p and m_t the masses of projectile and target, F_q the fraction of recoils in the selected charge state, and ϵ the stopping cross section of the target per atom per unit area (units of energy and area to match those of $\omega\gamma$ and λ^2).

4.1 Beam normalization

With stable beams, the integrated beam on target during a run was measured using Si detectors in the gas cell to count protons resulting from elastic scattering of beam ions with hydrogen nuclei in the target [1]. The elastic monitor response was calibrated against beam current measured in a Faraday cup lo-

cated upstream of the gas target, for each beam species and at each beam energy.

4.2 Target stopping power

The stopping powers were measured directly from the energy of the beam after the gas target, with and without gas in the target. Data obtained after the measurements reported in Table 1 of Ref. [18] lead to slight changes for the values we have adopted here.

4.3 Recoil ion charge state fractions

Charge state distributions were determined by direct measurement of recoil yields in different charge states, or from beams of the same atomic species as the recoils. With typical target thickness of 3×10^{18} atoms/cm^2, recoils from a resonant capture near the mid-point of the gas cell would reach charge state equilibrium [19] before exiting the target.

4.4 Separator acceptance

From simulation of the ion optics, it was expected that unscattered recoil ions originating on the optic axis at the centre of the target should be transmitted through the separator at angles up to 20 mrad. Non-zero beam spot size and divergence, as well as scattering in the gas, could reduce by several mrad the reaction cone angles at which losses would begin. However, for the reactions listed in Table 3 it was expected that essentially 100% of the recoil ions in the selected charge state would be transmitted to the detector at the end of the separator.

4.5 Detector efficiencies

At the lower beam energies, where the energy information from the Si strip detector did not cleanly distinguish recoil particles from leaky beam, it was necessary to tag recoils by requiring coincident detection of a gamma ray. The BGO array detection efficiency depends upon the gamma–decay scheme of the resonance, as well as the (hardware and software) energy thresholds. The BGO efficiency was estimated by GEANT simulation based on data using gamma–ray sources [20,21] and by comparing the ratio of recoil-gamma coincidence

rate to singles rate for events in a background-free region of the recoil energy spectrum. The two methods gave consistent results where direct comparison was possible for a simple decay scheme.

The double-sided Si strip detector which detected recoil ions had an estimated efficiency of 99±1% for analysis in which there was no software cut on pulse heights. When the analysis included a cut around the full-energy peak, the efficiency was reduced to 96.2±0.1% due to losses from hits between strips, which produced pulses of reduced amplitude [22,1].

4.6 Yields measured at DRAGON

Yields were measured for the reactions listed in Table 3. In most cases, yields were measured over a range of beam energies which spanned W, the energy thickness of the target (the average energy loss by beam ions that passed through the target). An example is shown in figure 6, where yields are calculated from the observed number of reactions, corrected for charge state fraction and recoil detector efficiency.

When the energy thickness of the target is much greater than the resonance width, Γ, the yield curve reaches a "plateau" of nearly constant values, the thick-target yield of Eq. 2. However, when Γ or the energy spread of the incident beam, σ_E, is comparable to W, the maximum yield is less than the thick-target yield. In the two reactions where $\Gamma \approx$ W the yields listed in Table 4 were further corrected (by "target factor") to thick-target yields, using a model which assumed a Gaussian beam energy spread, uniform energy loss through the target and a Breit-Wigner resonance lineshape.

Results presented in Ref. [2] were augmented by subsequent measurements of charge state fraction and BGO efficiency for the ^{21}Ne(p,γ)^{22}Na resonance at 258.6 keV, a run at double the gas pressure (8 Torr) for the 731.5 keV resonance and reduction of uncertainties in the stopping power and charge state fraction for the ^{20}Ne(p,γ)^{21}Na reaction. The resulting resonance strengths are presented in Table 4.

In view of the caveats concerning measurements of radiative capture strengths, there is reasonable agreement between our results and previous work. In ^{20}Ne(p,γ)^{21}Na, we disagree with the Ne gas target experiment of Thomas and Tanner [14] but are in good agreement with an experiment using a target of implanted ^{20}Ne [15]. For the ^{21}Ne(p,γ)^{22}Na resonance at 258.6 keV, the one case where the recoils approach the angular acceptance limit of the separator, our result for $\omega\gamma$ is larger than the one previous measurement by double the estimated measurement uncertainties. Finally, all three resonances in ^{24}Mg(p,γ)^{25}Al agree well with recent experiments.

5 CONCLUSIONS

Inverse kinematics plus a windowless gas target, γ array and recoil separator allows reliable determination of resonance energy. The targets are uniform, free of impurity layers and their thickness may be varied easily. Position of a narrow resonance within the gas target may be deduced from the pattern of hits in the γ array and stopping power of the target may be measured directly, enabling accurate extrapolation to beam energy at the resonance. A single measurement may be sufficient to establish a resonance energy to within a small fraction of the energy thickness of the target, an advantage when dealing with the low reaction rates in nuclear astrophysics experiments with unstable beams.

Beam suppression by the separator can vary by orders of magnitude (10^8 to 10^{13}), depending on the energy/mass ratio of the beam and the difference in mass/charge ratios of beam and the desired recoil ions. Future studies will focus on identifying causes of scatter in suppression factors.

The recoil ion detection system provides an additional beam suppression factor which depends upon the difference in atomic number and in the energy/mass ratio of the recoil ions compared to the beam ions. At low energies, a local time-of-flight measurement can provide useful rejection of the leaky beams typical of proton capture experiments.

Finally, the detection of γ rays in coincidence with recoil ions gives additional rejection by a factor of 10^5 or more for the stable beam reactions studied in this work.

Yield measurements with a gas target and inverse kinematics present a set of systematic uncertainties much different from those of solid target experiments in normal kinematics. Target properties are much better understood and controlled, while on the other hand the efficiency of the recoil separator and high-acceptance gamma detectors may be harder to understand than for the gamma detectors typically used in non-inverse kinematics. Comparison with previous measurements of capture strengths produced only one major discrepancy out of six cases. Given the historically-demonstrated difficulty in performing precision radiative capture experiments, the other five cases should be considered as a validation at the 15–20% level.

6 ACKNOWLEDGMENTS

We are grateful to TRIUMF staff and in particular to ISAC Operations crews and to R. Laxdal, K. Jayamanna, M. Pasini, Z. Peng and M. Marchetto for their work in providing accelerated stable beams. P. Machule and D. Preddy provided technical assistance; D. Lang, C. Neish, M. Anderson, A. Ruberg and K. Oraas assisted in collection and analysis of data. Financial support was received from the Natural Sciences and Engineering Research Council of Canada, from the U.S. Department of Energy (DE-FG03-93ER40789) and from the Deutsche Forschungsgemeinschaft (GR 1577/3-1).

References

[1] D. Hutcheon *et al.*, Nucl. Instr. and Meth. A498 (2003) 190.

[2] S. Engel, Ph.D. Thesis, Ruhr-Universität, 2003 and http://dragon.triumf.ca/docs/sabine_thesis.pdf.

[3] G. Audi, A.H. Wapstra and C. Thibault, Nucl. Phys. A729 (2003) 337.

[4] R. Bloch, T. Knellwolf and R.E. Pixley, Nucl. Phys. A123 (1969) 129.

[5] H.W. Becker *et al.*, Zeit. für Phys. A343 (1992) 361.

[6] S. Bishop *et al.*, Phys. Rev. Lett. 90 (2003) 162501.

[7] M. Mukherjee *et al.*, Phys. Rev. Lett. 93 (2004) 150801.

[8] G. Savard *et al.*, G. Savard et al., Phys. Rev. C70 (2004) 042501.

[9] D. Seweryniak *et al.*, Phys. Rev. Lett. 94 (2005) 032501.

[10] A. Anttila *et al.*, Zeit. für Phys. 234 (1970) 455.

[11] P.M. Endt, Nucl. Phys. A521 (1990) 1.

[12] J.M. D'Auria *et al.*, Phys. Rev. C69 (2004) 065803.

[13] M. Lamey, M.Sc. thesis, Simon Fraser University, 2004 and http://dragon.triumf.ca/docs/Lamey_thesis.pdf.

[14] G.C. Thomas and N.W. Tanner, Proc. Phys. Soc. 75 (1960) 498.

[15] J. Keinonen, M. Riihonen and A. Anttila, Phys. Rev. C15 (1977) 579.

[16] C. Angulo *et al.*, Nucl. Phys. A656 (1999) 3.

[17] D.C. Powell *et al.*, Nucl. Phys. A660 (1999) 349.

[18] U. Greife *et al.*, Nucl. Instr. and Meth. B217 (2004) 1.

[19] W. Liu *et al.*, Nucl. Instr. and Meth. A496 (2003) 198.

[20] D. Gigliotti, M.Sc. thesis, University of Northern British Columbia, 2004 and http://dragon.triumf.ca/docs/DarioThesis.pdf.

[21] D. Gigliotti, J. Rogers and A.H. Hussein, Nucl. Instr. and Meth. B204 (2003) 671.

[22] C. Wrede *et al.*, Nucl. Instr. and Meth. B204 (2003) 619.

Table 1
Calculated field-to-energy conversion constant, c_{mag} in (MeV/u)(T m)$^{-2}$, from measurement of (p,γ) resonances. The proton beam resonance energy, E_p, for ^{20}Ne(p,γ) is from Ref. [4]. For ^{21}Ne(p,γ) E_p is the average of resonances at 270.67 and 271.56 keV, weighted by $\omega\gamma$ [5].

Beam	E_p (keV)	q	B (T)	c_{mag}
^{20}Ne	1168.8(4)	8	0.38740(7)	48.21(3)
^{21}Ne	271.54(4)	4	0.39274(31)	48.09(8)

Table 2
Variation of charge-field product with MD1 field strength for a ^{24}Mg beam of fixed incident energy. Measurement uncertainties are estimated to be 0.03%.

q	B (T)	q·B (T)
3	0.536005	1.6080
4	0.401637	1.6065
5	0.321214	1.6061
6	0.267586	1.6055

Table 3
Stable beam reactions re-measured at DRAGON. E_{cm} is the centre-of-mass resonance energy, $\Phi_{1/2}$ is the cone half-angle of the recoils and $\omega\gamma$ is the resonance strength measured in previous experiments.

Reaction	$\Phi_{1/2}$ (mrad)	$E_{c.m.}$ (keV)	$\omega\gamma$ (meV)	Ref.
^{20}Ne(p,γ)^{21}Na	3.8	1112.6	1130(70)	[14]
			800(150)	[15]
^{21}Ne(p,γ)^{22}Na	14.9	258.6	82.5(12.5)	[16]
^{21}Ne(p,γ)^{22}Na	9.4	731.5	3950(790)	[16]
^{24}Mg(p,γ)^{25}Al	5.1	214.0	12.7(0.9)	[17]
^{24}Mg(p,γ)^{25}Al	4.0	402.2	41.6(2.6)	[17]
^{24}Mg(p,γ)^{25}Al	3.3	790.4	532(41)	[16]

Table 4. Reaction rates per incident beam particle, corrected for charge state fraction, recoil detector efficiency and (if required) BGO efficiency. These rates were converted to thick-target yields and combined with stopping powers to produce resonance strengths, $\omega\gamma_{DRA}$. Our measurements of resonance strength are compared to previous results, $\omega\gamma_{prev}$.

Reaction	E_{cm} (keV)	Selected charge state	Charge state fraction	BGO efficiency	Total Yield	Stopping power 10^{-15} eV·cm^2/at	Target factor	$\omega\gamma_{DRA}$ meV	$\frac{\omega\gamma_{DRA}}{\overline{\omega\gamma_{prev}}}$
^{20}Ne(p,γ)^{21}Na	1112.6	9+	0.59±0.01	—	(1.06±0.04)×10^{-9}	64.1±3.4	1.00	843±55	0.75±0.07 [14] 1.07±0.21 [15]
^{21}Ne(p,γ)^{22}Na	258.6	4+	0.57±0.05	0.44±0.02	(6.55±1.2)×10^{-10}	83.0±3.4	1.00	150±28	1.82±0.44
	731.5	8+	0.60±0.01	—	(4.88±0.17)×10^{-9}	86.9±5.6	0.90	3660±267	0.93±0.21
^{24}Mg(p,γ)^{25}Al	214.0	4+	0.34±0.05	0.42±0.04	(6.54±1.20)×10^{-11}	83.4±3.1	1.00	10.9±2.0	0.86±0.17
	402.2	6+	0.29±0.03	0.50±0.04	(1.14±0.16)×10^{-10}	110.0±4.7	1.00	48±7	1.15±0.18
	790.4	9+	0.41±0.02	—	(7.00±0.54)×10^{-10}	105.0±3.7	0.94	584±50	1.10±0.13

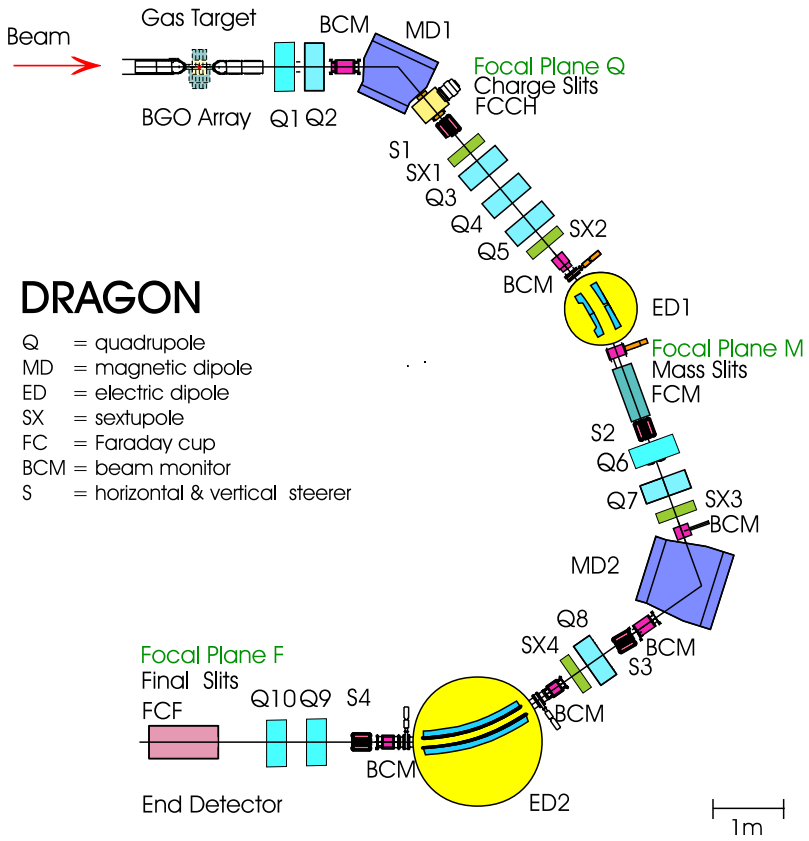

Fig. 1. Schematic view of the DRAGON facility.

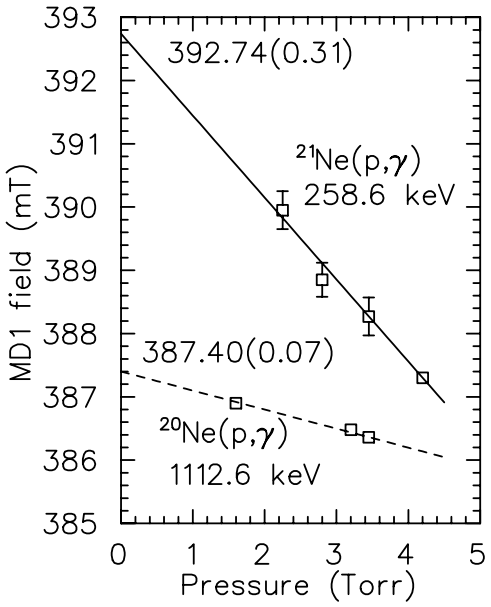

Fig. 2. Determination of the MD1 magnet constant by extrapolation to zero pressure in the gas target cell.

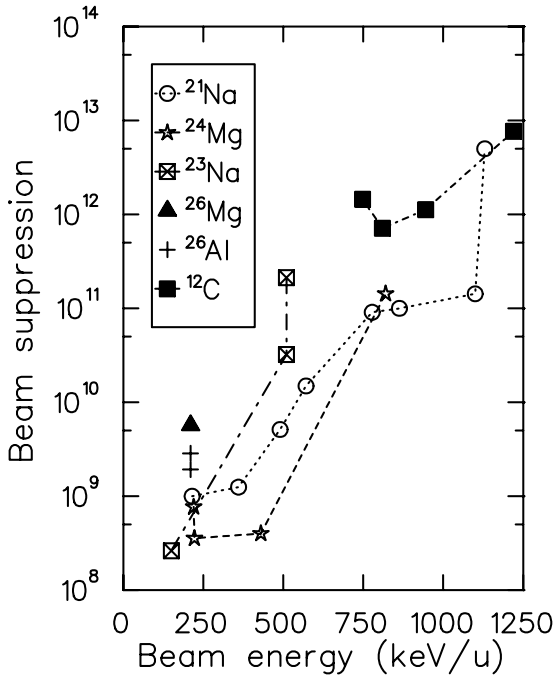

Fig. 3. Beam suppression by the DRAGON mass separator for various beams. The separator was tuned for recoils from proton capture, except for the ^{12}C case which was tuned for alpha capture. The vertical and horizontal slits at the final focus position were open to 45 mm in each direction. The selected charge state at a given energy was the most-probable state for recoil ions.

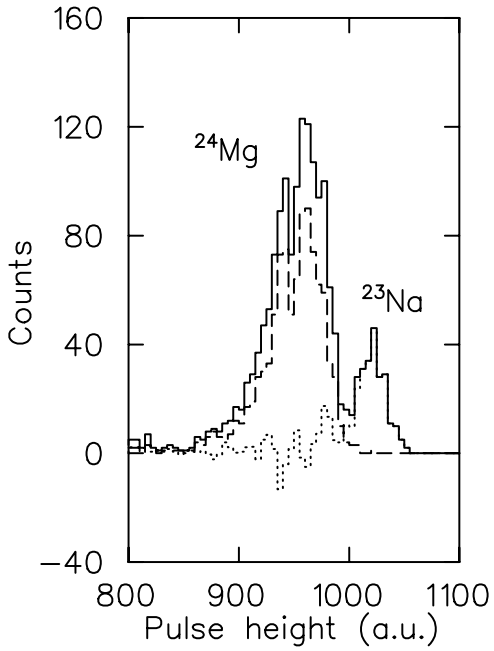

Fig. 4. Beam rejection by the double-sided silicon strip detector. The observed spectrum (solid line) consists of the recoil ^{24}Mg ions from the ^{23}Na(p,γ) resonance at 508 keV/u and a peak to the right consisting of transmitted beam ions. Counts in the dashed-line histogram are in coincidence with gamma rays. The dotted-line spectrum is the residual attributed to beam, after dividing the coincidence counts by gamma detection efficiency and subtracting from the total.

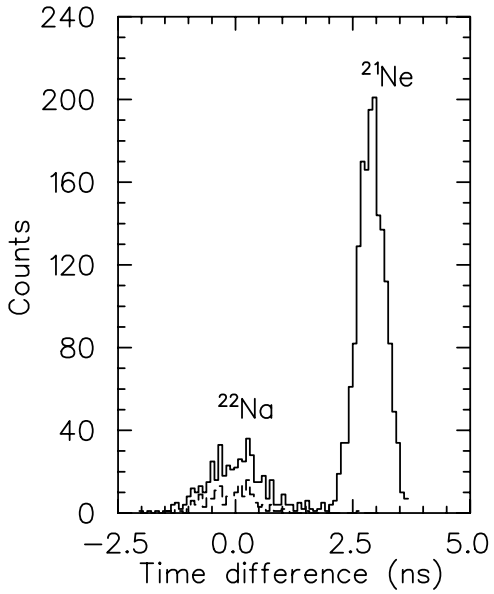

Fig. 5. Separation of leaky beam from recoils for the ^{21}Ne(p,γ)^{22}Na resonance at 269 keV/u using time-of-flight (TOF), with times calculated as a difference from the nominal TOF for recoils. The dashed-line histogram shows the subset of particles that were in coincidence with gamma rays. The Start signal came from a micro-channel plate detecting secondary electrons from a C foil and the Stop signal from a plastic scintillator and photo-multiplier tube. The flight path was 43 cm long.

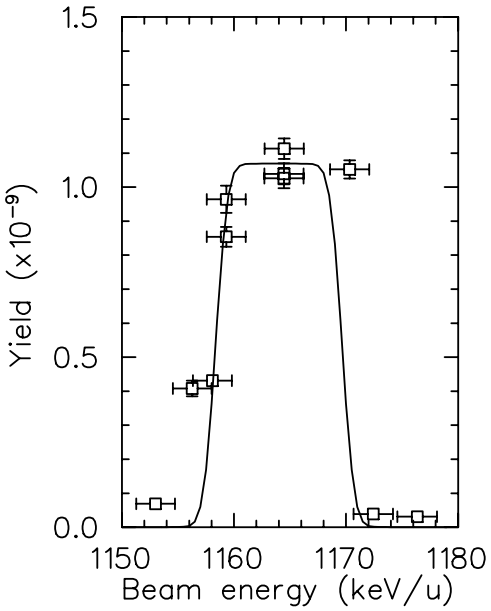

Fig. 6. Yield per incident beam ion vs beam energy for the ^{20}Ne(p,γ)^{21}Na resonance at 1112.6 keV. The curve is a double-arctangent form (target thickness 11.2 keV/u and natural width 0.015 keV/u) folded with a Gaussian beam energy distribution (2 keV/u FWHM).